Anal Bioanal Chem (2014) 406:5369–5378
DOI 10.1007/s00216-014-7900-y

RESEARCH PAPER

Preparation of QP4VP-*b*-LCP liquid crystal block copolymer and its application as a biosensor

Muhammad Omer · Soo-Young Park

Received: 2 January 2014 / Revised: 12 May 2014 / Accepted: 14 May 2014 / Published online: 1 July 2014

Abstract The interface between nematic liquid crystal, 4-cyano-4′-pentylbiphenyl (5CB), and water in a transmission electron microscopy (TEM) grid cell coated with QP4VP-*b*-LCP (quaternized poly(4-vinylpyridine) (QP4VP) and poly(4-cyanobiphenyl-4′-oxyundecylacrylate) (LCP)) was examined for protein and DNA detection. QP4VP-*b*-LCP was synthesized by reversible addition-fragmentation chain transfer (RAFT) polymerization. Quaternization of P4VP with iodomethane (CH_3I) made it a strong cationic polyelectrolyte and allowed QP4VP-*b*-LCP to form complexes with oppositely charged biological species. Several proteins, such as bovine serum albumin (BSA), hemoglobin (Hb), α chymotrypsinogen-A (ChTg), and lysozyme (LYZ), were tested for nonspecific protein detection. By injecting the protein solutions into the TEM grid cell, the initial homeotropic orientation of the TEM grid cell changed to a planar orientation above their isoelectric points (PIs) due to electrostatic interactions between QP4VP (+charge) and proteins (−charge), which did not occur below the PIs of the tested proteins. Their minimum concentrations at which the homeotropic to planar configurational change (H-P change) occurred were 0.01, 0.02, 0.03, and 0.04 wt.% for BSA, ChTg, Hb, and LYZ, respectively. One of the strong anionic polyelectrolytes, deoxyribonucleic acid (DNA) (due to the phosphate deoxyribose backbone) was also tested. A H-P change was observed with as little as 0.0013 wt.% salmon sperm DNA regardless of the pH of the cell. A H-P change occurred in 5CB and was observed by polarized optical microscopy. This simple and inexpensive setup for nonspecific biomaterial detection provides the basic idea for developing effective selective biosensors by introducing specific binding groups, such as the aptamer and antibody.

Keywords Strong cationic polyelectrolyte · QP4VP-*b*-LCP · Protein · DNA · RAFT polymerization · Biosensor

Introduction

Over the past two decades, block copolymers (BCPs) have been studied extensively for the formation of nanostructures in the solution or bulk state arising from the incompatibility of the two blocks [1]. Appropriate selection of the nature of each block during the synthesis steps of a BCP determines its final applications. For example, the hydrogen-bonding capability of the poly(4-vinylpyridine) (P4VP)-containing BCPs imparted the valuable properties of binding some important species, which led to the formation of new nanostructures [2]. Among the other functional units in BCPs, charge-carrying units impart functionality to interact with other useful charged species through electrostatic interactions. In the biological fields, protein and DNA detection is used widely to diagnose some diseases in patients, which require sophisticated instruments or expensive sensors. Laborious labeling of these biological species is sometimes needed, which might change their original properties. Therefore, certain methods have been devised in which protein is made intact and being detected without any damage to the protein [3–6]. Recently, newly developed liquid crystal (LC)-based sensors omitted extra steps for labeling and allowed the use of the cheapest instruments in this field [7–9]. LCs are sensitive to a range of stimuli, such as temperature, electric and magnetic fields, and shear [10]. Orientation anchoring of the LC molecules

Electronic supplementary material The online version of this article (doi:10.1007/s00216-014-7900-y) contains supplementary material, which is available to authorized users.

M. Omer · S.-Y. Park (✉)
Department of Polymer Science, Kyungpook National University, #1370 Sangyuk-dong, Buk-gu, Daegu 702-701, South Korea
e-mail: psy@knu.ac.kr

relative to the interface arranges them either in the perpendicular (homeotropic) or parallel (planar) states. Transitions between these two states at the LC/water interface can be modulated by functional materials that can bind the target biomaterials. Polarized optical microscopy (POM) can reveal the orientational changes that occur in LC mesogens. The direct introduction of these functional materials (e.g., adsorption) at the LC/water interface is undesirable because long-term stability is necessary to respond to the interactions with the detecting species. Because of the polymerizability of the LC mesogens and its compatibility with used LC molecules, a BCP in which liquid crystalline polymer (LCP) is linked covalently to a functional polymer is a better choice for the fixation of functional materials at the LC/water interface because the LCP block can penetrate easily into 4-cyano-4′-pentylbiphenyl (5CB) due to its compatibility with LC molecules, and provide support for the functional polymer at the LC/aqueous interface.

Polyelectrolytes can be used for functional materials at the LC/water interface. Polyelectrolytes are of fundamental interest in daily life because they also have the properties of both polymers and electrolytes. These charged macromolecules have attracted considerable interest to biochemists and biologists because polyelectrolytes are involved in many biological phenomena. Biopolyelectrolytes include proteins, salts of deoxyribonucleic acid (DNA), hyaluronic acid, heparin, alginic acid, pectinic acid, carboxymethyl cellulose, etc.; synthetic polyelectrolytes include poly(styrenesulfonate), poly(acrylic acid), poly(vinylalcohol sulfate), etc. Polyelectrolytes can be cationic or anionic depending on the charge state of the pendant group. They can also be strong or weak. Strong polyelectrolytes have permanent charges and are ionized over the entire pH range, whereas weak polyelectrolytes can only be ionized in a limited pH range. Sodium poly(styrene sulfonate) (PSS) and poly(diallyldimethylammonium chloride) (PDADMAC) are examples of a strong polyanion and polycation, respectively, and polyallylamine hydrochloride (PAH) and polyacrylic acid (PAA) are a weak polycation and polyanion, respectively [11]. PAA-*b*-LCP, as a functional material, was used for the first time to show the response of the LC orientation to the pH of the solution [12] and protein detection in minute quantities using both a TEM grid cell and microdroplets prepared by microfluidics [13]. The responses for the TEM grid cell and microdroplets were the homeotropic-to-planar (H-P) and radial-to-bipolar changes, respectively. On the other hand, there was a certain pH range to induce electrostatic interactions between the PAA chains and charged biomaterials because PAA is a weak anionic polyelectrolyte and can be deprotonated above its pK_a (~4.7) to have a negative net charge. If the target material is a protein, the pH in the protein solution should also be considered because the charge state of the protein is dependent on its isoelectric point (PI) in that the total net charge is positive and negative below and above its PI, respectively. Therefore, the pH range between the pK_a of PAA and the PI of the protein can induce electrostatic interactions. In particular, the protein with a low PI requires a low pH to have a positive charge so that the protein is denatured in such an acidic medium. To utilize the polyelectrolyte for use over a wide range of pH, strong polyelectrolytes that are independent on the pH for the charged state are necessary.

In this article, a novel quaternized amphiphilic diblock copolymer, QP4VP-*b*-LCP, was synthesized by addition-fragmentation chain transfer (RAFT) polymerization and a quaternization reaction with iodomethane (CH_3I) to make it a strong polyelectrolyte, and the TEM grid cell was used as a platform for protein and DNA detection. Functionalization of the TEM grid cell with QP4VP was achieved by transfer of the QP4VP-*b*-LCP monolayer on the 4-cyano-4′-pentylbiphenyl (5CB, nematic LC at room temperature) in a TEM grid cell using a Langmuir Blodgett (LB) trough. The performance of this TEM grid cell was examined for nonspecific protein and DNA detection with bovine serum albumin (BSA), hemoglobin (Hb), α chymotrypsinogen-A (ChTg), and lysozyme (LYZ) as well as salmon sperm DNA via a H-P change by POM under crossed polarizers. The effects of the pH in the TEM cell and the pI of the tested proteins on protein detection were screened to examine the H-P change through electrostatic interactions between the protein (and DNA) and QP4VP. Strong electrostatic interactions between them caused a H-P change at the several hundred nanomolar level. This study might provide fundamental information on the role of the strong polyelectrolyte in the LC-based biosensors, and on the design of a specific protein detection system through this convenient, label-free, and inexpensive detection method using selective protein detection units, such as antibodies and aptamers.

Experimental

Materials 4-Vinylpyridine monomer (4-VP, Aldrich) was purified by passing through an alumina column to remove the inhibitor, and azobis (isobutyronitrile) (AIBN, Junsei) was recrystallized from a benzene/hexane (1/2, *v*/*v*) mixture and washed with methanol. *N*,*N*-dimethylformamide (DMF, Aldrich), 5CB (TCI, 100 %), diethyl ether (Duksan), octadecyltrichlorosilane (OTS), phenylmagnesium bromide, tetrahydrofuran (THF), 4-cyano-4′-hydroxybiphenyl, 11-bromo-1-undecanol, methanol, potassium hydroxide, acryloyl chloride, triethylamine, carbon disulfide, methyl α-bromophenylacetate, iodomethane, diethyl ether, and anhydrous magnesium sulfate were used as received. All water used in this study was purified using a Millipore Milli-Q system, and the resistivity was >16 MΩ cm, and the pH buffer solutions (Samchun©, Korea) were used as received. Copper

specimen grids (G75, with a grid hole width of 285 μm, pitch of 340 μm, bar width of 55 μm, and rim width of 0.225 mm) were supplied by Gilder Grids (UK). LYZ was purchased from MP Biomedicals, and salmon fish DNA, BSA, Hb, and ChTg were supplied by Aldrich.

Synthesis of the chain transfer agent of the MCPDB and LC11 monomer The chain transfer agent (CTA), *S*-methoxycarbonylphenyl-methyl dithiobenzoate (MCPDB) was prepared using the method reported by Perrier et al. [14, 15] as shown in Scheme 1. Briefly, a solution of phenylmagnesium bromide (3.49 mL) in THF (28 mL) was heated to 50 °C and carbon disulfide (1.58 mL, 26.0 mmol) was added dropwise over approximately 20 min to produce a dark brown solution. Methyl α-bromophenylacetate (1.37 mL, 8.7 mmol) was then added to the solution. The reaction temperature was raised to 80 °C and maintained at that temperature for 13 h. Ice water was then added to the solution before extracting the organic products three times with diethyl ether. The combined organic extracts were rinsed with water and dried over anhydrous magnesium sulfate. After removing the solvent, column chromatography was performed in dichloromethane and *n*-hexane mixture (2/1, *v*/*v*) to obtain an orange red oil (52.4 %).

4-Cyanobiphenyl-4′-oxyundecylacrylate (LC11) monomers were prepared according to the procedures reported in the literature, as shown in Scheme 2 [16, 12]. LC11 monomers were synthesized by the etherification of 4-cyano-4′-hydroxybiphenyl (4.02 g, 20.62 mmol) and 11-bromo-1-undecanol (5.23 g, 20.80 mmol). 11-Bromo-1-undecanol was added dropwise to a methanol solution (40.01 mL) of 4-cyano-4′-hydroxybiphenyl and potassium hydroxide (1.38 g, 24.67 mmol), and then the mixture solution was heated under reflux for 25 h. After the reaction, the product was recrystallized twice from methanol (yield, 65 %). After recrystallization, the compound was treated with triethylamine (0.40 mL, 2.84 mmol) and acryloyl chloride (0.23 g, 2.45 mmol) to yield a mesogenic monomer. After stirring for 16 h at room temperature, LC11 was purified by recrystallization from methanol twice (yield, 45 %) [15]. Figures S1 and S2 (Electronic supplementary material) show the ^{1}H-nuclear magnetic resonance (NMR) spectra of MCPDB and LC11, respectively. Every peak in the spectra was assigned to the protons in both compounds in terms of the position and integrated area.

Synthesis of macroinitiator (P4VP-MCPDB) Scheme 3 shows the RAFT polymerization scheme for the synthesis of the macroinitiator, P4VP-MCPDB. 4-Vinylpyridine (4-VP) (1.068 mL), MCPDB (CTA) (5.49 mg, 0.018 mmol), and DMF (1.115 mL) were added to a graduated vial and the mixture solution was bubbled with dry nitrogen for 60 min. A Schlenk flask containing AIBN (0.596 mg, 0.00363 mmol) was vacuumed for 60 min and the previously prepared mixture solution of 4-VP and CTA in DMF was then introduced into the flask using a syringe needle purged with N_2 before. The flask was placed in an oil bath at 80 °C for 4 h for the RAFT reaction. The resulting macroinitiator, P4VP-MCPDB, was precipitated in diethyl ether. The number average molecular weight (M_n) and polydispersity index (PDI) of the homopolymer were 47.6 K and 1.24, respectively. Volatile materials were removed in the vacuum at 40 °C to yield a dried pink color powder. The origin of the pink color is the end group of MCPDB. Figure SI 3 shows the ^{1}H-NMR data of P4VP-MCPDB and P4VP-*b*-LCP along with the protons and integrated area.

Synthesis of QP4VP-b-LCP Scheme 3 shows the overall reaction scheme for the synthesis of QP4VP-*b*-LCP. To synthesize P4VP-*b*-LCP via the RAFT method, AIBN (0.34 mg, 0.0021 mmol), LCP (88.04 mg, 0.2099 mmol) and P4VP–MCPDB (199.84 mg, 0.0042 mmol) were added to a Schlenk flask. A toluene/ethanol mixture (4/6, *v*/*v*, 3.037 mL) [17] was poured into the Schlenk flask and the solution was degassed by bubbling N_2 gas for 60 min. The flask was placed in an oil bath thermostated at 65 °C for 6 h. After the reaction was complete, the product was precipitated in diethyl ether. Volatile materials were removed in a vacuum at 40 °C to yield yellowish powders. The M_n and PDI of the P4VP-*b*-LCP were 53.8 and 1.23 K, respectively. P4VP-*b*-LCP (0.062 g) was dissolved in DMF (5 mL), and CH_3I (0.186 mL) was then added dropwise into the polymer solution at 0 °C in darkness. This reaction continued at 20 °C for 16 h with stirring. When the reaction was finished, the mixture was added dropwise to an excess of ethyl ether and the product was precipitated, filtered, and dried in a vacuum oven at 40 °C to remove the unwanted volatile components completely.

Preparation of TEM grid cell and the flow chamber The glass slides were first cleaned using a piranha solution (H_2SO_4/H_2O_2 mixture (70/30, *v*/*v*)). A piranha solution reacts violently with organic materials and should be handled with extreme care; it should not be stored in closed containers. The glass slides were heated in the piranha solution for 30 min at 80 °C, rinsed sequentially with water, ethanol, and methanol, dried under N_2 purging, immersed into an OTS solution at 40 °C for 30 min, rinsed again with methylene chloride, and finally dried under N_2 purging. The TEM grid cells and flow chambers were prepared using the procedures reported in the literature [12]. Figure 1 shows a schematic diagram for the preparation of the flow chamber used in this study. The glass microscope slides were cleaned using published procedures and coated with OTS [18]. Copper specimen grids (cleaned sequentially with methylene chloride, ethanol, and methanol) were placed on the surface of the small OTS-coated glass substrates, which was glued onto another glass slide with epoxy (Fig. 1a). A small volume of 5CB (~1 μL) was

Scheme 1 Synthesis of MCPDB (CTA)

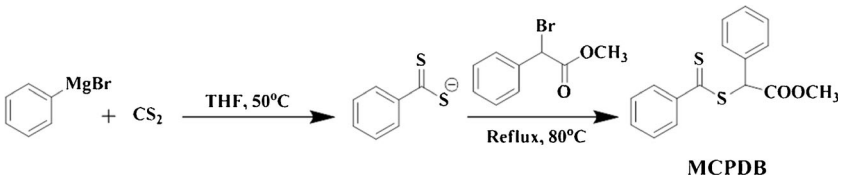

dispensed onto each grid by dropping, and the excess 5CB was removed by placing a narrow capillary tube in contact with the TEM grid. The thickness of the 5CB layer on the TEM grid was approximately 20 μm. QP4VP-*b*-LCP (0.8 wt.%) was dissolved in a THF/water mixture (1/1, *v*/*v*) for LB film formation. The QP4VP-*b*-LCP solution (0.5 mL) was spread on the water in the LB bath to prepare the monolayer, and the surface pressure of the monolayer was controlled at 60 mN/m using a LB trough to obtain a constant brush density. After successful monolayer formation on the water surface (Fig. SI 5), the prepared TEM grid cell was inserted slowly (TEM grid side down) into the LB bath on the silicon spacer attached to another glass slide, which was already placed in the LB bath (Fig. 1b). The two glass slides (which were separated by a silicon spacer) were clipped with binding clips. Inlet and outlet ports for exchanging solvents were made by hypodermic needles that pierced the silicon spacer (Fig. 1c).

Characterization Fourier transform infrared (FT-IR, Jasco FT/IR-620, Japan) spectroscopy was performed using potassium bromide (KBr) pellets with a resolution of 4 cm^{-1}. The samples for FT-IR spectroscopy were vacuum dried in an oven at 40 °C to remove moisture. A small quantity of the sample with KBr salt was ground to obtain a homogenous mixture and pressed into a FT-IR pellet. The molar masses and molar mass distributions were determined by gel permeation chromatography (GPC) using a PLgel Organic GPC column and RI750F refractive index detector (Young Lin Instrument Co., Acme 9000, Korea). DMF was used as the eluent with a flow rate of 0.8 mL min^{-1} and calibration was carried out using polystyrene standards (Aldrich Chemical Co., USA). The ^1H nuclear NMR spectra were obtained at ambient temperature with a 400 MHz Bruker spectrometer (Germany) using deuterated chloroform ($CDCl_3$) as the solvent for P4VP-MCPDB and P4VP-*b*-LCP, and deuterated dimethyl sulfoxide (DMSO-d_6) for QP4VP-*b*-LCP. The optical photographs were obtained through a polarized optical microscope (Samwon, LSP-13, Korea) equipped with crossed polarizers [12].

Results and discussion

Synthesis of QP4VP-b-LCP Figure SI 4 shows GPC traces of the homopolymer (P4VP-MCPDB) and block copolymer (P4VP-*b*-LCP). The increase in the molecular weight of P4VP-*b*-LCP compared to P4VP-MCPDB can be observed clearly. The molecular weight of P4VP-*b*-LCP was P4VP (47.6 K)-*b*-LCP (6.2 K) with a PDI of 1.23.

Figure 2 shows the ^1H NMR spectrum of QP4VP-*b*-LCP. Each peak position, their respective integrated area, and number of protons are as follows: δH (d_6-DMSO): 2.49–2.51 (a, m, 14H, $(-CH_2)_7$), 2.53–2.55 (b, c, m, main chain, 4H, $-CH_2$), 2.56–2.58 (a′, m, 4H, $-CH_2$), 2.73–2.89 (d, m, 1H, −CH), 3.3–3.7 (e, m, 1H, −CH), 4.18–4.37 (f, g, h, 7H, $-OCH_2$, CH_3), 7.87–8.15 (i, j, k, m, 8H, aromatic), and 8.76–8.79 (l, m, 4H aromatic). The peak at 3.3 ppm represents the protons of water in the deuterated DMSO. d_6-DMSO always contains water. The peaks were assigned to the protons in the chemical structure, indicating that block copolymerization occurred via RAFT polymerization.

Figure 3 shows the FT-IR spectra of P4VP, P4VP-*b*-LCP, and QP4VP-*b*-LCP. The FT-IR spectrum of the P4VP homopolymer showed characteristic stretching vibration peaks at 1,415, 1,600, 2,927, and 3,024 cm^{-1} for the pyridine ring, C=C, CH_2, and C=CH, respectively. These peaks were also observed in the spectrum of the P4VP-*b*-LCP along with new peaks at 1,494 and 2,225 cm^{-1} for the phenyl ring, and C≡N stretching vibrations of the LCP block, respectively. This also indicates successful block copolymerization. Quaternization of the block copolymer was confirmed by the decrease in peak

Scheme 2 Synthesis of the LC11 monomer

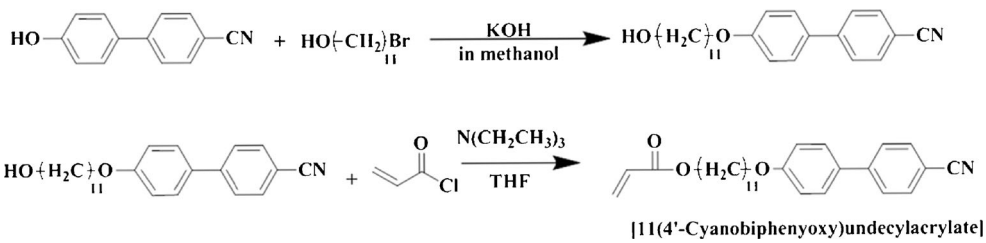

Scheme 3 Synthesis of QP4VP-*b*-LCP via RAFT polymerization

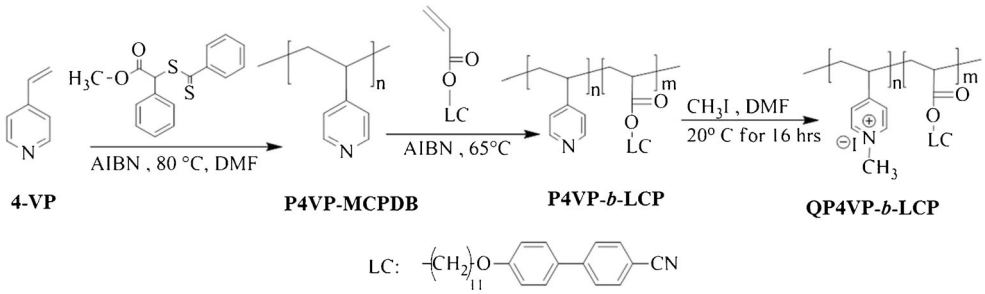

intensity at 1,412 cm^{-1} (C=C stretching vibration) in the spectrum of QP4VP-*b*-LCP compared to that of P4VP-*b*-LCP, and the appearance of a new peak at 1,638 cm^{-1} due to the quaternized pyridine rings with a methyl group. The small peak at 2,762 cm^{-1} and the broad peaks at 3,400 and 3,414 cm^{-1} in the spectrum of QP4VP-*b*-LCP were assigned to –N(CH_3) in the pyridine ring and intermolecular hydrogen bonding with its neighboring molecules, respectively. The degree of quaternization of the P4VP blocks was calculated by the intensity ratio between the in-plane stretching band of the charged pyridinium ring at 1,638 cm^{-1} and that of the neutral pyridinium ring at 1,600 cm^{-1}. The percentage quaternization with ordinary alky halide (CH_3I) was ~74.2 % [19, 20].

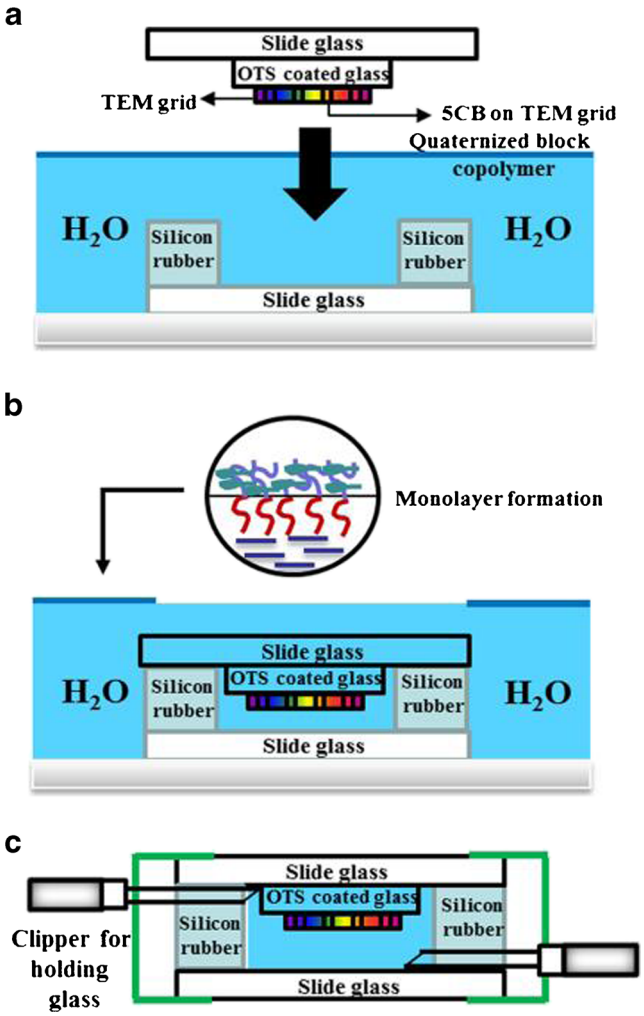

Fig. 1 Schematic diagrams of the flow chamber used for protein and DNA detection; the TEM grid cell in the flow chamber **a** before and **b** after QP4VP-*b*-LCP was coated on the 5CB; **c** final TEM cell with inlet and outlet ports

Protein detection BSA, Hb, ChTg, and LYZ were examined as model proteins for protein detection. The pIs of BSA, Hb, ChTg, and LYZ are 4.7, 6.8, 8.9, and 11.35, respectively, according to the Sigma-Aldrich product information sheet. Figure 4a shows the POM images of the functionalized TEM grid cell with QP4VP-*b*-LCP (TEM_{QP4VP} grid cell) under crossed polarizers after injecting different pH solutions, ranging from 2 to 12 with and without proteins. All images without proteins had a homeotropic orientation regardless of the pH in the cell, indicating that the cationic charges of QP4VP on 5CB induced the perpendicular orientation of 5CB against the LC/water interface. This homeotropic orientation of the TEM_{QP4VP} grid cell regardless of pH in the cell has merit because a homeotropic orientation is the reference state for protein detection through a H-P orientational change so that the possible pH range for protein detection was widened. The PAA-*b*-LCP functionalized TEM (TEM_{PAA}) grid cell in a previous report had a certain pH range for a homeotropic orientation. After injecting BSA, Hb, ChTg, and LYZ solutions (0.01, 0.04, 0.03, and 0.05 wt.%, just above the critical concentration for the H-P change, which will be discussed in the following section in this article) at different pHs, the initial homeotropic orientation did not change below the pIs of all proteins tested (in the positive charge state), whereas it changed to a planar orientation above them (in the negative charge state). Therefore, this H-P orientational change might be due to complexation between the protein and QP4VP through electrostatic interactions.

Figure 4b shows the POM images of the TEM_{QP4VP} grid cell after injecting protein solutions at pH 7, 9, 10, and 12 for BSA, Hb, ChTg, and LYZ, respectively, at different protein concentrations of 0.005 to 0.06 wt.%. The pH of the tested protein solution was chosen above its pI to have a negative net charge. The minimum protein detection limits through the H-P change were observed at 0.01, 0.03, 0.02, and

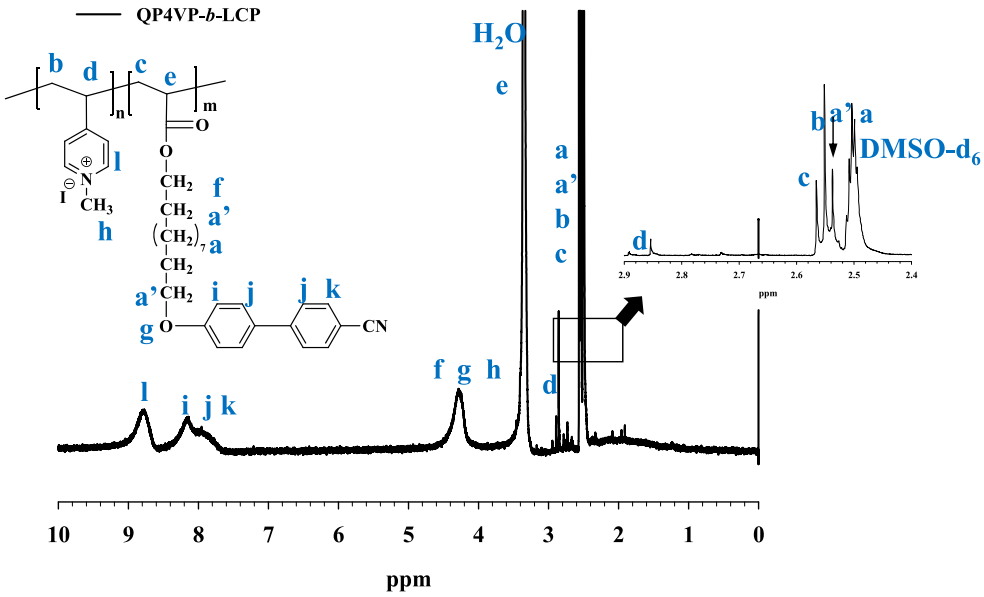

Fig. 2 ^{1}H-NMR spectrum of QP4VP-*b*-LCP with the peak assignments

0.04 wt.% for BSA, Hb, ChTg, and LYZ, respectively. If the weight percent were converted to the mole concentration, there are several hundred nanomolar levels. These low detection limits suggest that the cationic strong polyelectrolyte of QP4VP could bind the proteins strongly via electrostatic interactions. The adsorption of proteins can occur in many ways, such as electrostatic interactions, hydrophobic interactions, hydrogen bonding, etc. These results suggest that an electrostatic interaction is a major mechanism for protein detection in polyelectrolyte LC-based biosensors.

In order to confirm the complexation between BSA and QP4VP, 0.1 wt.% of BSA labeled with FITC was injected to the TEM_{QP4VP} grid cell at pH 3, 6, and 9 (Fig. 4c (i), (ii), and (iii), respectively) and then the TEM_{QP4VP} grid cell was washed with PBS water having the same pH, to observe whether the detachment of proteins occurs or vice versa. The green color was

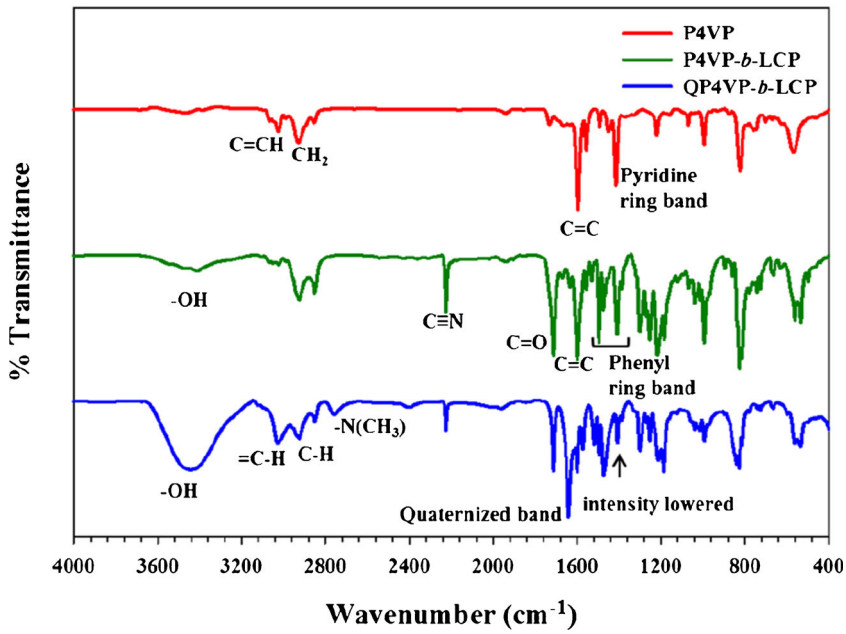

Fig. 3 FT-IR spectra of P4VP, P4VP-*b*-LCP, and QP4VP-*b*-LCP

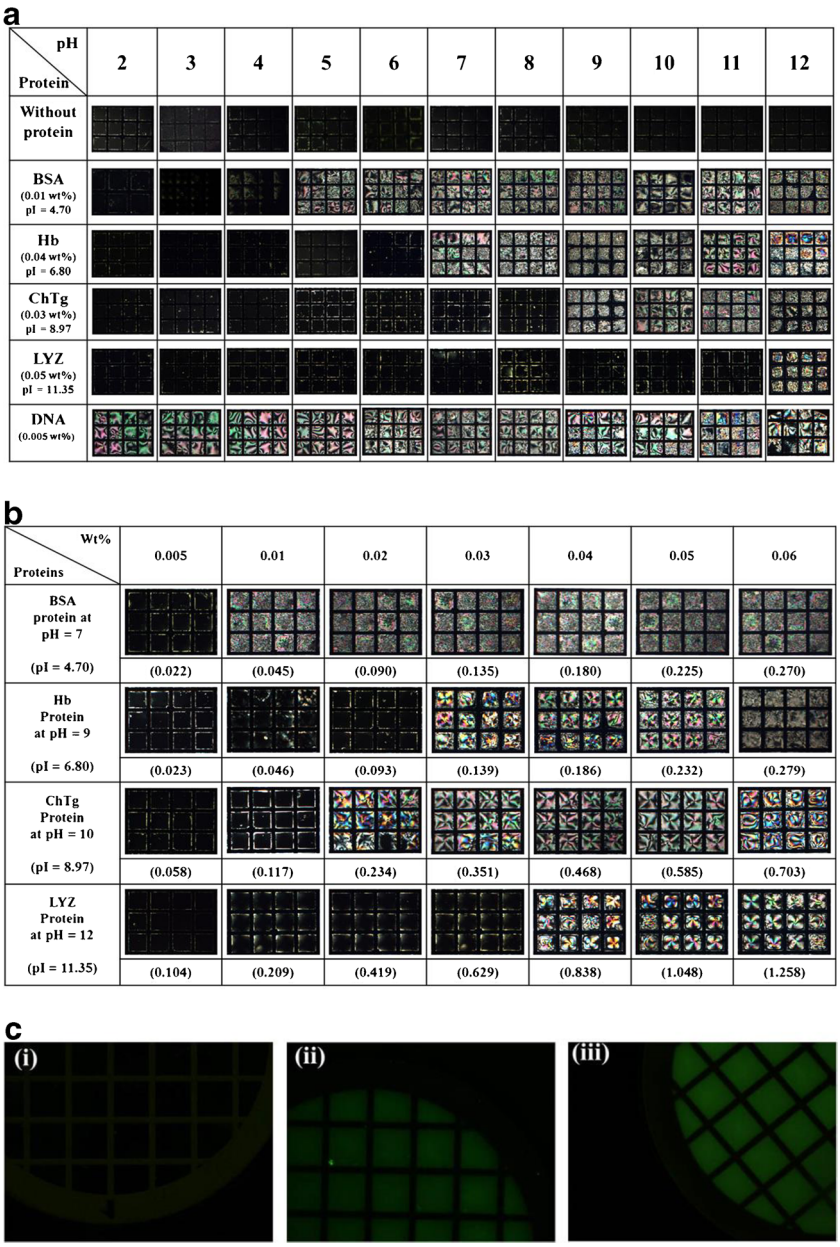

Fig. 4 POM images of the TEM_{QP4VP} grid cell without and with proteins under cross-polarizers **a** at the pH range, 2 to 12, with protein and DNA concentrations of 0.01, 0.04, 0.03, 0.05, and 0.005 wt.% for BSA, Hb, ChTg, LYZ, and salmon fish DNA, respectively, and **b** at the different concentrations of 0.005 to 0.06 wt.% with pHs of 7, 9, 10, and 12 for BSA, Hb, ChTg, and LYZ, respectively; the *numbers in parentheses* indicate μM. **c** fluorescent images of the TEM grid cells after injecting a FITC-BSA (0.1 wt.%) solution at pHs of (*i*) 3, (*ii*) 6, and (*iii*) 9

observed in the region of the TEM grids at pH 6 and 9, although the black image was observed at pH 3 indicating that the negatively charged FITC-BSA had made electrostatic interactions with the oppositely charged polymer at pH 6 and 9, while no protein adsorption happened at pH 3 due to the same charges between

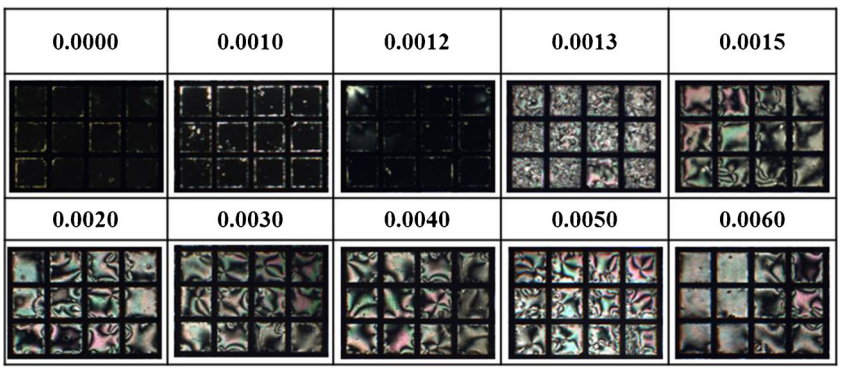

Fig. 5 POM images of the TEM grid cells in a cross-polar state after injecting salmon fish sperm DNA at different concentrations; the *number in the graph* represents the weight percent of the aqueous DNA solution at pH 7

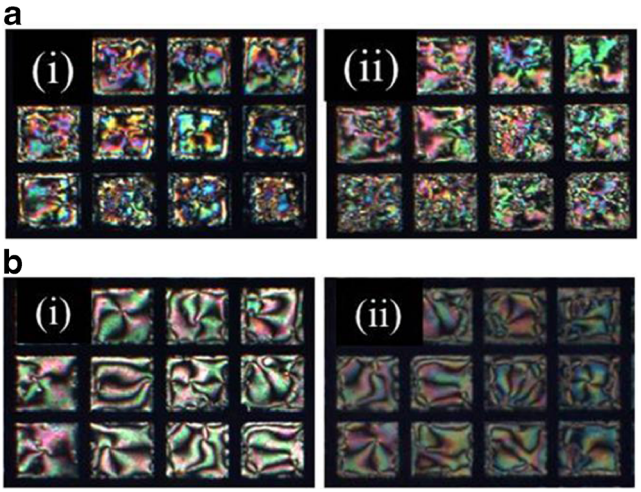

Fig. 6 POM images of the TEM_{QP4VP} grid cells under crossed polarizers (*i*) before and (*ii*) after washing with water; **a** the 0.01 wt.% Hb solution at pH 9 and **b** the 0.06 wt.% ChTg solution at pH 10 were injected into the cell before washing with the aqueous pH 9 and 7 solutions, respectively

them. All the experiments in Fig. 4a–c were performed at the individual cells made at different pHs and protein concentrations.

Thus, this result clearly indicates that the complex formation occurred through electrostatic interactions which induced the orientational change of 5CB in the TEM grid. The reason why this orientational change happened as a result of complex formation may be a decrease in electrical field toward the neutral state of the complex although a detailed study is necessary for its mechanism.

DNA detection Figure 5 shows POM images of the TEM_{QP4VP} grid cell after injecting salmon fish sperm DNA solutions at different concentrations until 0.006 wt.% in a pH 7 buffer solution. DNA was soluble in the aqueous medium and negative charged because of the phosphate deoxyribose backbone. The initial homeotropic orientation changed to the planar orientation at 0.0013 wt.% by complexation between the negative-charged DNA and positive-charged QP4VP, similar to electrostatic interactions with the negative net-charged proteins. The detection limit of DNA was lower than those of the proteins tested in Fig. 4. This lower detection limit might be due to the stronger negative charge compared to those of the proteins because every nucleotide unit has a negative phosphate deoxyribose group in DNA. The pH dependency of DNA detection was also tested. Figure 4a (last row) presents POM images of the TEM_{QP4VP} grid cell with DNA (0.005 wt.%, above the critical concentration) under cross-polarizers at the pH range, 2 to 12. The initial homeotropic orientation changed to a planar orientation at pHs of 2 to 12, indicating that the TEM_{QP4VP} grid cell could detect DNA regardless of the pH of the solution. DNA is a strong polyelectrolyte so that the charge state of the DNA is not dependent on the pH. Therefore, complexation between strong cationic (QP4VP) and anionic (DNA) polyelectrolytes through electrostatic interactions is possible regardless of the pH in the solution.

Stability and reversibility Hb and ChTg were selected as model proteins to confirm the stability and reversibility of the TEM_{QP4VP} grid cell for protein and DNA detection. To test the stability of the TEM_{QP4VP} grid cell for protein detection, the TEM_{QP4VP} grid cell was first injected with a 0.01 wt.% Hb solution at pH 9 and then washed with the pH 9 buffer aqueous solution without a protein. Washing with water was performed by injecting 3 mL water in the cell to

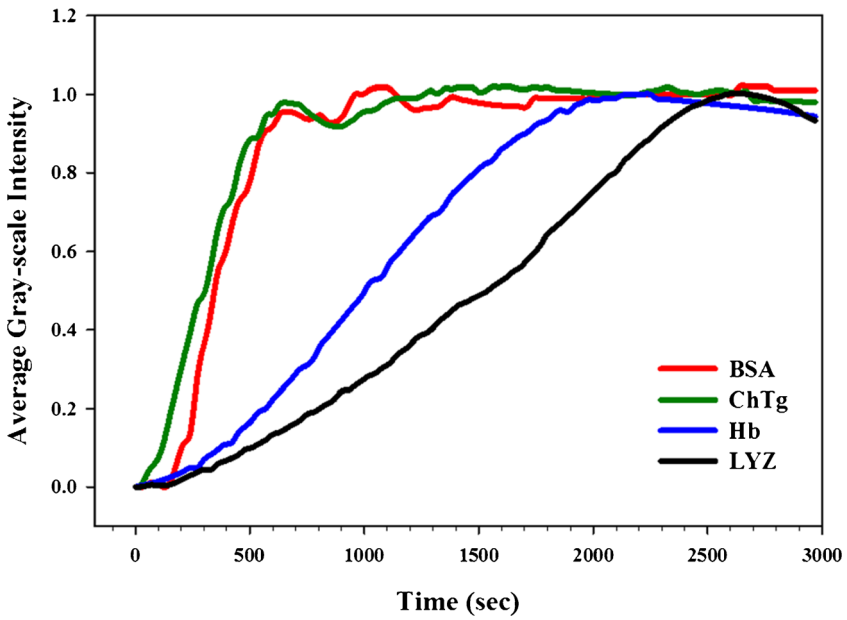

Fig. 7 Change in the GI after injecting BSA (0.04 wt.%), ChTg (0.04 wt.%), Hb (0.05 wt.%), and LYZ (0.06 wt.%) solutions into the TEM grid cell at pH 7, 10, 9, and 12, respectively

replace the aqueous medium in the cell with a volume of 0.6 mL. Figure 6a shows POM images of the TEM_{QP4VP} grid cells under crossed polarizers before and after washing with water. The initial planar orientation by complexation between Hb and QP4VP did not change after washing with water suggesting that complexation was strong enough to be maintained during washing. The reversibility of the TEM_{QP4VP} grid cell for protein detection was also tested by changing the pH in the cell. The main mechanism for protein detection is the electrostatic interactions between the proteins and QP4VP. This electrostatic interaction can be controlled by the pH because the charge state of the protein can change with the pH depending on its PI. The TEM_{QP4VP} grid cell was first injected with a 0.06 wt.% ChTg solution at pH 10, and then washed with a pH 7 buffer aqueous solution without a protein. As shown in Fig. 4, the ChTg solution caused the planar and homeotropic orientations in the TEM_{QP4VP} grid cell at pH 10 and 7, respectively. The planar orientation at pH 10 was attributed to complexation between the protein and QP4VP. On the other hand, the planar orientation at pH 10 did not change after injecting a pH 7 aqueous solution, as shown in Fig. 6b, indicating that complexation still remained after changing the medium pH to 7. The ChTg had a total net positive charge at pH 7 because of its PI of 8.97 so that the electrostatic interactions appeared to be difficult to form at this pH. Several possible reasons can explain the irreversibility of the protein adsorption by changing the pH above and below its PI. One of them is that the charged state of the already contacted part in the protein with QP4VP by electrostatic interactions could not be altered by changing the pH in the medium due to the strong interactions. Another reason might be that the protein still contained negative-charged groups, even when the pH of the protein solution was lower than its PI because the PI represents the relative amounts of negative and positive pendant groups, i.e., more positive groups than the negative groups (not all positive groups) at lower than its PI.

Detection speeds of protein and DNA Figure 7 shows the change in the mean gray-scale intensity (GI) with time after injecting BSA, Hb, ChTg, and LYZ solutions in the TEM_{QP4VP} grid cell at pH 7, 9, 10, and 12 with their respective concentrations of 0.04, 0.04, 0.05, and 0.06 wt.%, respectively. The concentration and pH were chosen just above the detection limits (Fig. 4b) and their PI, respectively. The GI increased gradually and became saturated with time due to the H-P orientational change through the formation of a complex between the proteins and QP4VP. The times for reaching half saturated intensity were 240, 283, 998, and 1,290 s for BSA, Hb, ChTg, and LYZ, respectively. They are longer than the values (several seconds) observed from the TEM_{PAA} grid cell [21]. This slow complexation in the TEM_{QP4VP} grid cell might be because the mechanism for the TEM_{PAA} grid cell involved a change in the chain conformation of the PAA chains, which did not occur on the TEM_{QP4VP} grid cell. Nevertheless, more study will be needed for further clarification using other dynamic tests, which are out of the scope in the present work.

Conclusions

A novel QP4VP-*b*-LCP was synthesized via RAFT polymerization and quaternization of P4VP with CH_3I and demonstrated its potential as a biosensor for nonspecific protein and DNA detection. A monolayer of QP4VP-*b*-LCP constructed through a LB trough was transferred to the surface of a TEM grid filled with 5CB as a detecting layer. Complexation between the protein and QP4VP occurred above the PI of the protein, and was detected via a change in 5CB alignment from a homeotropic to planar configuration. The detection limits for BSA, Hb, ChTg, and LYZ were 0.045, 0.139, 0.234, and 0.838 μM, respectively. Salmon fish sperm DNA could also be detected using this TEM_{QP4VP} grid cell, regardless of the pH in the cell because it had negative charged phosphate deoxyribose groups along the chain and a strong anionic polyelectrolyte. The detection limit was 0.0013 wt.% in a pH 7 buffer solution, which was much lower than the tested proteins. This simple and inexpensive setup for nonspecific biomaterial detection provides the basic idea for developing effective selective biosensors by introducing specific binding groups, such as aptamers, antibodies, single-stranded DNA, proteins, peptides, and aptamer-binding RNA on the cell [12].

Acknowledgments This work was supported by the National Research Foundation of Korea (NRF-2011-0020264).

References

1. Hamley IW, Castelletto V (2004) Small-angle scattering of block copolymers in the melt, solution and crystal states. Prog Polym Sci 29:909–948
2. Yeh SW, Wei KH, Sun YS, Jeng US, Liang KS (2005) CdS nanoparticles induce a morphological transformation of poly(styrene-*b*-4-vinylpyridine) from hexagonally packed cylinders to a lamellar structure. Macromolecules 38:6559–6565
3. Seong HC, Chang HS, Kwang PL (2005) Preparation for protein separation of an ion-exchange polymeric stationary phase presenting amino acid and amine units through surface graft polymerization. Macromol Res 13:39–44
4. Kyung WK, Hyun C, Gil SL, Dong JA, Min-K O (2006) Micropatterned polydiacetylene vesicle chips for detecting protein-protein interactions. Macromol Res 14:483–485
5. Sehoon J, Ui SK, Wonjin J, Chee BS (2009) Fabrication of multicomponent protein microarrays with microfluidic devices of poly(-dimethylsiloxane). Macromol Res 17(No. 3):192–196

6. Lee E, Kim J, Myung J, Youngjong K (2012) Modification of block copolymerphotonic gels for colorimetric biosensors. Macromol Res 20(No. 12):1219–1222
7. Brake JM, Daschner MK, Luk YY, Abbott NL (2003) Biomolecular interactions at phospholipid-decorated surfaces of liquid crystals. Science 302:2094–2097
8. Skaife JJ, Abbott NL (2001) Influence of molecular-level interactions on the orientations of liquid crystals supported on nanostructured surfaces presenting specifically bound proteins. Langmuir 17:5595–5604
9. Skaife JJ, Brake JM, Abbott NL (2001) Influence of nanometer-scale topography of surfaces on the orientational response of liquid crystals to proteins specifically bound to surface-immobilized receptors. Langmuir 17:5448–5457
10. Jerome B (1991) Surface effects and anchoring in liquid crystals. Rep Prog Phys 54:391–451
11. York AW, Kirkland SE, McCormick CL (2008) Advances in the synthesis of amphiphilic block copolymers via RAFT polymerization: stimuli-responsive drug and gene delivery. Adv Drug Deliv Rev 60:1018–1036
12. Lee DY, Seo JM, Khan W, Kornfield JA, Kurji Z, Park SY (2010) pH-responsive aqueous/LC interfaces using SGLCP-*b*-polyacrylic acid block copolymers. Soft Matter 6:1964–1970
13. Khan W, Park SY (2012) Configuration change of liquid crystal microdroplets coated with a novel polyacrylic acid block liquid crystalline polymer by protein adsorption. Lab Chip 12:4553–4559
14. Perrier S, Takolpuckdee P, Westwood J, Lewis DM (2004) Versatile chain transfer agents for reversible addition fragmentation chain transfer (RAFT) polymerization to synthesize functional polymeric architectures. Macromolecules 37:2709–2717
15. Khan W, Seo JM, Park SY (2011) Synthesis and micellization of a novel diblock copolymer of poly(*N*-isopropylacrylamide)-*b*-SGLCP and its application in stability of 5CB droplets in aqueous medium. Soft Matter 7:11549
16. Dubois JC, Decobert G, Barny PL, Friedrich SC, Noel C (1986) Liquid crystalline side chain polymers derived from poly-acrylate, poly-methyacrylate and poly-α-chloroacrylate. Mol Cryst Liq Cryst 137:349–364
17. Bozovic-Vukic J, Manon HT, Meuldijk J, Koning C, Klumperman B (2007) SAN-*b*-P4VP block copolymer synthesis by chain extension from RAFT-functional poly(4-vinylpyridine) in solution and in emulsion. Macromolecules 40:7132–7139
18. Yang JY, Mathauer Frank CW (1994) Microchemistry: spectroscopy and chemistry in small domains. In: Tamai N (ed) Masuhara H, FC Kitamura. North Holland, New York
19. Bicak N, Gazi M (2003) Quantitative quaternization of poly(4-vinyl pyridine). J Macromol Sci-Pure Appl Chem A40:585–591
20. Sonmez HB, Bicak N (2002) Quaternization of poly(4-vinyl pyridine) beads with 2-chloroacetamide for selective mercury extraction. React Funct Polym 51:55–60
21. Seo JM, Khan W, Park SY (2012) Protein detection using aqueous/LC interfaces decorated with a novel polyacrylic acid block liquid crystalline polymer. Soft Matter 8:198–203